THE ASTROPHYSICAL JOURNAL, 552:877–888, 2001 May 10

BLUE LINES AS CHROMOSPHERIC DIAGNOSTICS: THE Si I LINES AT 3906 AND 4103 Å

CAROLINA CINCUNEGUI AND PABLO J. D. MAUAS[1]
Instituto de Astronomía y Física del Espacio (IAFE), Casilla de Correo 67, Sucursal 28, Buenos Aires 1428, Argentina
Received 2000 October 2; accepted 2001 January 16

ABSTRACT

We present a complete atomic model for Si I line synthesis. We study how the computed profiles of two blue lines of this atom are influenced by the choice of the atomic parameters and find that, although several cross sections are not known accurately, the line profiles do not depend strongly on them and are therefore useful as diagnostics of the atmospheric structure. We study which transitions need not be included in the model, in order to reduce as much as possible the computing time. We compare the profiles computed for a standard model of the quiet solar atmosphere with the observations and find very good agreement. We confirm that irradiation by UV lines originating in the transition region above sunspot umbrae or plages strongly enhances the continuum between 1300 and 1700 Å, which is due to Si I bound-free transitions. If line fluxes typical of the impulsive phase of flares are assumed, the line profiles are also affected.

Subject headings: atomic processes — line: formation — line: profiles — stars: chromospheres — Sun: chromosphere

On-line material: machine-readable table

1. INTRODUCTION

One of the most successful ways to study the structure of the solar chromosphere has been the construction of semiempirical models. This technique has become a mature one, in particular from the benchmark works by Vernazza, Avrett, & Loeser (1973, 1976, 1981), which built what can be now considered the standard model of the quiet solar chromosphere. This model was slightly modified later in the $T_{\min}$ region by Avrett (1985). This technique was also applied to the study of different features in the Sun, from sunspots (Maltby et al. 1986) to flares (Machado et al. 1980; Mauas, Machado, & Avrett 1990; Mauas 1993), and to the models of different types of cool stars (e.g., Cram & Mullan 1979; Giampapa, Worden, & Linsky 1982; Thatcher, Robinson, & Rees 1991; Houdebine & Doyle 1994; Mauas & Falchi 1994, 1996; Mauas et al. 1997). For "semiempirical" we mean that, given a T-versus-z distribution, the non-LTE populations for hydrogen, and perhaps other species, are computed, solving simultaneously the equations of hydrostatic equilibrium, radiative transfer, and statistical equilibrium.

Once the calculations are completed for a particular atmospheric model, the emerging profiles for a given set of lines are computed, and the results are compared with the observations. Then the assumed T-versus-z distribution is modified, until a satisfactory match between the observations and the prediction of the calculations is obtained. However, there are several intrinsic problems regarding this approach. The most important lies in the uniqueness of the models computed in this way. In other words, knowing that a particular atmosphere would emit a line profile like the observed one does not imply that the atmosphere indeed has this structure, since we do not know whether some other atmosphere would produce the same profile.

This problem is, of course, larger when the modeling is based only in matching a small number of spectral features. For example, the indetermination is larger when the only thing to be matched is the Hα profile than when the Ca II K line is also used (let alone when only line fluxes, or even Balmer decrements, are used as diagnostics, instead of the whole line profile).

As part of an ongoing project of constructing atmospheric models for cool stars, in a recent paper (Mauas 2000) we studied how changes in the assumed chromospheric structure of dM and dMe stars affect the emitted spectrum. In this way, we study if a given set of features can wholly determine the atmospheric structure, how large are the indeterminations in the atmospheric parameters deduced, and to what extent the atmospheric model computed can be considered unique. We find that the profiles of the Ca II K line or the Na D lines can be used to determine the structure of the $T_{\min}$ region, and the Hα profile can provide good information on the structure of the chromosphere. The Lyα flux, in turn, can be used to constrain the position of the transition region. However, it is not always possible to obtain simultaneous profiles for lines far apart in the spectrum, as a result of observational constraints. Therefore, it is desirable to find lines in the same spectral region that can provide information on the atmospheric structure. In particular, one of the most observed spectral regions is the one around the H and K lines of Ca II, since these lines are the most widely used indicators of chromospheric activity, in both the Sun and other cool stars. For example, Cauzzi et al. (1995; see also Cauzzi et al. 1996), during a coordinated campaign, observed a solar flare that occurred on 1991 June 7. Their observations included spectra obtained with the Universal Spectrograph (USG) at the Vacuum Tower Telescope of the National Solar Observatory, Sacramento Peak, in the range 3500–4200 Å.

This spectral range is typical of other solar instruments as well. For example, the Blue Light Imaging Spectrograph (BLISP), which has been built by the Institute of Applied

[1] Member of the Carrera del Investigador Científico, CONICET, Argentina; carolina@iafe.uba.ar.

Physics of the University of Bern and has been operative for several years in Locarno, Switzerland, has a spectral range from 3700 to 4400 Å. BLISP has now been installed in the El Leoncito Observatory, in the Argentinean Andes, and we plan to use it extensively to observe different solar features.

The observations by Cauzzi et al. (1995) were used by Falchi & Mauas (1999), to build atmospheric models for the strongest kernel of this flare, based on the profiles of the Ca II K line and of Hδ, which are the strongest emission lines in the observed spectra (apart from Hϵ and Ca II H, which are blended). These are the first semiempirical models of a solar flare that consistently include the velocity fields observed. However, models based on only two spectral lines can be underconstrained, and it would be desirable to include other lines in the modeling. In particular, one of the strongest lines in this spectral region, which shows an emission core during the flare, is the one of Si I at 3905 Å. This line was already used by Cauzzi et al. (1996) to estimate the velocity fields during the observed flare.

Before this line, and another weaker Si I line at 4103 Å, can be used to check the semiempirical models, it is necessary to build an accurate atomic model, compiling the available atomic data, computing the parameters not available in the literature, and checking how much influence the possible inaccuracies in the parameters might have on the computed atmospheric model.

On the other hand, if this atomic model will be used to compute models with velocity fields, it is important to find a model with the smallest number of levels and transitions that still retains all the important physics. This is due to the fact that, when the Doppler effects are included, the number of frequency points at which the calculations have to be done is multiplied by the number of height points in the grid, and therefore the computing time increases by a large factor.

The physical conditions in Si I in the quiet solar atmosphere were studied by Vernazza et al. (1976, hereafter VAL76), who found that the UV line emission coming down from the corona causes as much as 15% of the photoionization of the Si I ground level, and therefore the UV continuum is only weakly coupled to the local electron temperature.

This fact was further studied by Machado & Hénoux (1982) and Machado & Mauas (1986), who found that the increments observed during flares in the continuum radiation at $\lambda < 1682$ Å, originated by Si I, are not due to temperature enhancements in the $T_{\min}$ region, where this continuum is originated, but to an increase in the UV line radiation from the transition zone during the flare. This fact was later confirmed observationally by Doyle & Phillips (1992). However, these studies were done with a very simplified atomic model, which is not appropriate to study the formation of the lines of interest here. The objective of this paper is, therefore, to study the atomic parameters of Si I and to build a reliable model with the lowest possible number of transitions and levels.

In § 2 we discuss the atomic parameters available in the literature. In § 3 we study the effect of the different levels on the ionization equilibrium and on the emitted profiles. In § 4 we present the "optimum model," i.e., the one that includes all the important processes, with the smallest number of transitions. In § 5 we check how much the computed profiles change when the atomic parameters are modified, to estimate the reliability of our atomic model. In § 6 we study the influence that the irradiation by UV lines coming down from the transition region has on the profiles and on the continuum below 1682 Å. Finally, in § 7 we discuss the results.

2. ATOMIC PARAMETERS

We have used an atomic model including 21 levels, which is shown in Figure 1. In Table 1 we list the designation and ionization wavelength of each level, together with the ionization rates discussed below. The previous papers used the model presented by VAL76, which included models 1–7 of the present work, and an eighth level consisting of the combination of our levels 10, 11, and 12. We consider that this model is complete enough to include all the levels and transitions needed to compute the populations of each level, and thus we will refer to it as the "complete model." In this section we present the atomic data we have used and discuss their uncertainties.

Asplund (2000) determined a solar Si I abundance relative to hydrogen of 3.236×10^{-5} or, in the usual logarithmic scale where the abundance of hydrogen is set to 12, a value of 7.51. Here we adopt the value given by Grevesse et al. (1991), of 3.548×10^{-5}, consistent with the abundances adopted for all other metals. We have performed a calculation with Asplund's value and found no differences in the computed profiles for the 3906 and 4103 Å lines.

2.1. *Bound-Free Cross Sections*

As discussed in Machado & Mauas (1986) and references therein, the ionization balance of Si I is strongly affected by the transition region UV lines irradiating the low chromosphere and $T_{\min}$ region. Therefore, very accurate photoionization cross sections are needed to account for these effects, since particular resonances can be fundamental to determine the Si I populations.

In this paper we use the cross sections by A. K. Pradhan & S. N. Nahar (2001, in preparation), as given by the TOPbase database at the CDS (Cunto et al. 1993). These theoretical values include all the resonances and are therefore much more detailed than the ones used in the former calculations quoted above. In Figure 2 we show the values used here for several levels and compare them with those used by VAL76 and in subsequent papers. As can be seen, there are very large differences between both sets of rates. Even when the rates at threshold are similar, as is the case for levels 2 and 6, the functions used in former papers ignore the very strong resonances, largely underestimating the cross sections at other wavelengths.

Regarding the threshold values, in Table 1 we include the ones adopted here and those given by VAL76. It can be seen that there are large differences for all levels, with the exception of level 2. In particular, the value for the ground level adopted here is twice as large as the one used by all the former authors. Unfortunately, as far as we are aware there are not more modern measurements to confront with, and we preferred to use the set of values given by A. K. Pradhan & S. N. Nahar (2001, in preparation) because they represent a coherent set of values that gives not only the values at threshold but also the dependence of the cross sections with wavelength.

The collisional ionization rate per atom in level l is given by

$$C_{lk} = n_e \Omega_l(T) \exp\left(\frac{-h\nu_{kl}}{kT}\right). \quad (1)$$

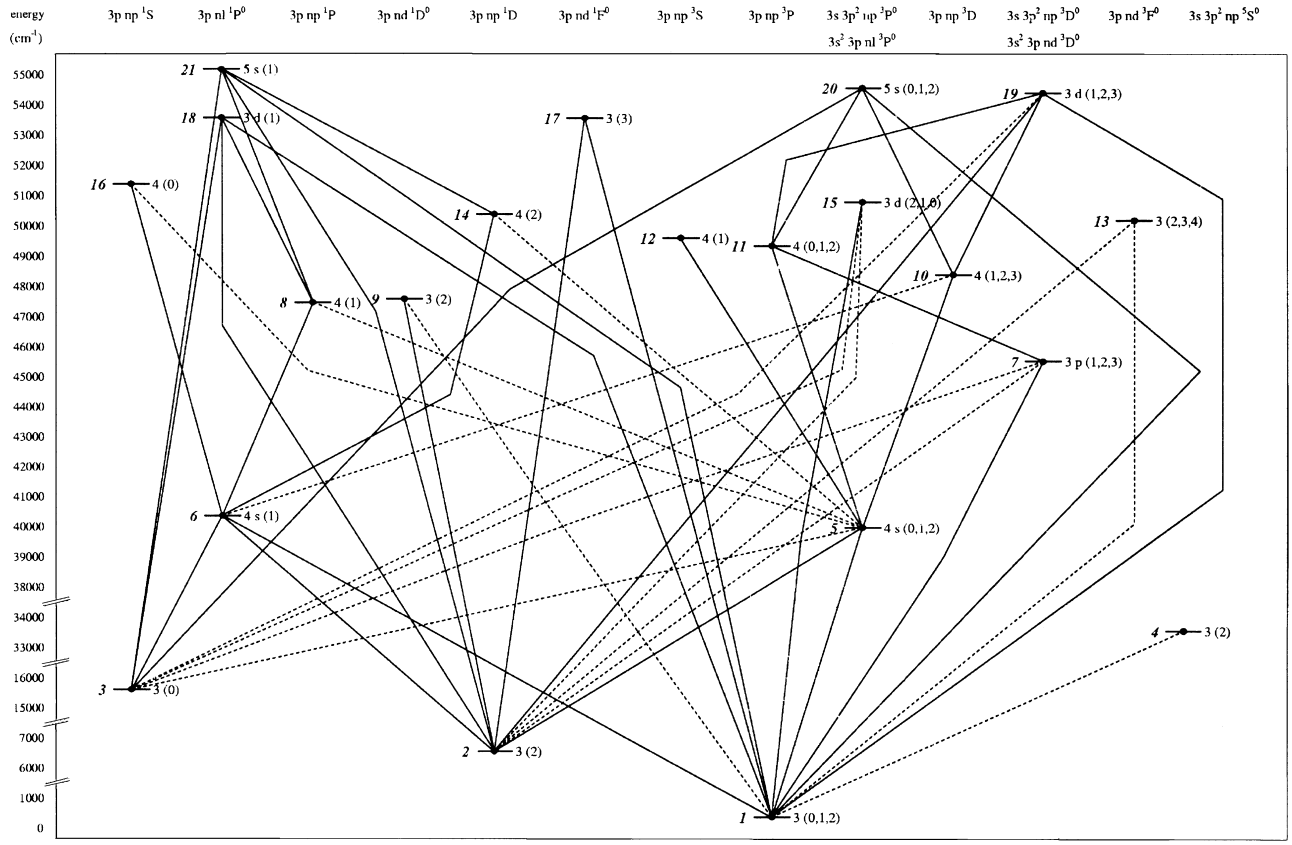

FIG. 1.—Energy level diagram of the atomic model. The solid lines indicate radiative transitions between the levels included in the optimum model, and dashed lines indicate transitions included only in the complete model.

The adopted values for $\Omega_l(T)$ at 3000, 5000, 7000, and 9000 K are listed in Table 1. We adopted the values given by VAL76 for the levels included in their work, and for the remaining ones we use a constant value of 10^{-7} cm^3 s^{-1}. Integration of the measured cross sections given by Freund et al. (1990) for the ground state gives Ω_1 values about 20% smaller than the ones we use. As the collisional ionization and recombination rates are much smaller than the corre-

TABLE 1

ATOMIC PARAMETERS FOR BOUND-FREE TRANSITIONS

						Ω_l (cm^3 s^{-1})			
l	DESIGNATION	λ_l (Å)	g_l	α_0 (mbar)	α_0 (VAL76)	3000 K	5000 K	7000 K	9000 K
1	$3s^23p^2\ ^3P$	1520	9	70.10	37.00	1.73(−8)	2.41(−8)	3.11(−8)	3.83(−8)
2	$3s^23p^2\ ^1D$	1682	5	34.60	35.00	1.90(−9)	2.70(−9)	3.54(−9)	4.42(−9)
3	$3s^23p^2\ ^1S$	1980	1	26.30	46.00	4.50(−8)	5.39(−8)	6.46(−8)	7.60(−8)
4	$3s3p^3\ ^5S^0$	3071	5	54.00	15.00	1.57(−8)	2.13(−8)	2.58(−8)	2.94(−8)
5	$3s^23p4s\ ^3P^0$	3832	9	0.56	1.25	2.62(−9)	3.51(−9)	4.20(−9)	4.74(−9)
6	$3s^23p4s\ ^1P^0$	4016	3	3.39	4.09	0.93(−8)	1.23(−8)	1.46(−8)	1.64(−8)
7	$3s3p^3\ ^3D^0$	4855	15	16.60	18.00	4.86(−8)	6.29(−8)	7.28(−8)	8.04(−8)
8	$3s^23p4p\ ^1P$	5374	3	39.10	...	1.00(−7)			
9	$3s^23p3d\ ^1D^0$	5393	5	15.70	...	1.00(−7)			
10.....	$3s^23p4p\ ^3D$	5629	15	22.20	14.10	1.00(−7)			
11.....	$3s^23p4p\ ^3P$	5952	9	46.10	14.10	1.00(−7)			
12.....	$3s^23p4p\ ^3S$	6063	3	5.23	14.10	1.00(−7)			
13.....	$3s^23p3d\ ^3F^0$	6271	21	16.40	...	1.00(−7)			
14.....	$3s^23p4p\ ^1D$	6368	5	36.40	...	1.00(−7)			
15.....	$3s^23p3d\ ^3P^0$	6520	9	19.50	...	1.00(−7)			
16.....	$3s^23p4p\ ^1S$	7002	1	28.40	...	1.00(−7)			
17.....	$3s^23p3d\ ^1F^0$	7980	7	28.60	...	1.00(−7)			
18.....	$3s^23p3d\ ^1P^0$	7996	3	29.60	...	1.00(−7)			
19.....	$3s^23p3d\ ^3D^0$	8563	15	10.30	...	1.00(−7)			
20.....	$3s^23p5s\ ^3P^0$	8672	9	2.02	...	1.00(−7)			
21.....	$3s^23p5s\ ^1P^0$	9072	3	4.80	...	1.00(−7)			

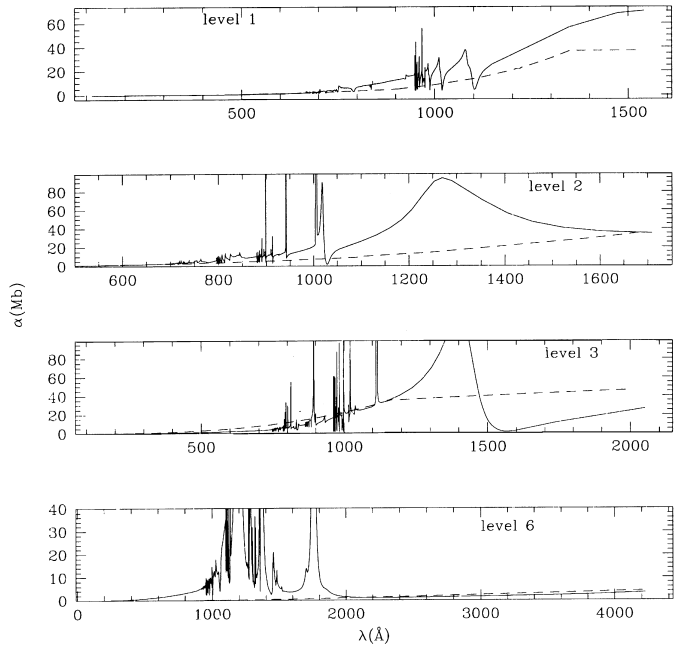

FIG. 2.—Photoionization cross sections for several levels (*solid line*). The dashed lines represent the values used by VAL76.

sponding radiative rates, we feel that it is not necessary to use more accurate data.

2.2. *Bound-Bound Cross Sections*

We considered all the allowed transitions between the 21 levels of our atomic model. For the Einstein coefficient A_{ul} we adopted the values of the NIST compilation[2] by Wiese & Fur (1999), when available, since this is a critical compilation of the best values available in the literature. For the remaining transitions, we adopted the experimental values by O'Brien & Lawler (1991) and Smith et al. (1987) or the ones given by the Vienna Atomic Line Database (VALD; Kupka et al. 1999; Ryabchikova et al. 1999; Piskunov et al. 1995), in that order. These values are listed in Table 2.

There are large differences between the values listed in the literature. For example, the transition 5–1 of our model is the multiplet 1 for Si I. Most measurements give values around $A_{51} = 1.7 \times 10^8$ s^{-1} (Savage & Lawrence 1966; Hoffmann 1969; Smith et al. 1987; Saloman 1990), which was adopted in the compilation by Morton (1991), and the NIST compilation gives a value of 1.74×10^8 s^{-1}. However, the more recent measurement by O'Brien & Lawler (1991) gives a value of 2.22×10^8 s^{-1}, which is 40% larger than the other measurements. This larger value is in agreement with the theoretical calculations by Hibbert (1979), Mendoza & Zeippen (1988), Mukherjee & Ohno (1989), Iglesias, Rogers, & Wilson (1992), Nahar (1993), and Nahar & Pradhan (1993) and with the compilation by Verner, Barthel, & Tytler (1994). The calculations by Ganas (1999), on the other hand, give the smallest value of all: $A_{51} = 1.5 \times 10^8$ s^{-1}. However, since these calculations are based on a less accurate model, we adopted the value measured by O'Brien & Lawler (1991), which is the most recent experimental result and is in agreement with most theoretical values.

The same situation is repeated for other lines. For example, the line 15–1 of our model has measured values of A_{15-1} ranging from 5.22×10^7 s^{-1} (Hoffman 1969) to 8.33×10^7 s^{-1} (O'Brien & Lawler 1991) and theoretical computations up to 5.45×10^8 s^{-1} (Mukherjee & Ohno 1989). Here we use the O'Brien & Lawler (1991) value.

For the 6–3 line, the value of 1.18×10^7 s^{-1} adopted here, from NIST and VALD, is the minimum value found in the literature, since O'Brien & Lawler (1991) give a value of 1.33×10^7 s^{-1}, Becker et al. (1980) of 1.43×10^7 s^{-1}, and Smith et al. (1987) of 1.5×10^7 s^{-1}.

Somewhat more complex is the situation of the weaker 5–3 line. O'Brien & Lawler (1991) and Smith et al. (1987) give only upper limits for this line, of 1.5 and 3.4×10^5 s^{-1}, respectively. Here we adopted the NIST value of 5.33×10^4 s^{-1}, compatible with this upper limit, although much lower than it. VALD gives an even smaller value of 3.2×10^4 s^{-1}.

We could not find in the literature any value for A_{13-1}. We have therefore adopted a value of 10^5 s^{-1} for this parameter. We will see below that this value is not important, since the line has no influence on the statistical equilibrium of the atom.

Also shown in Table 2 are line half-widths at half-maximum for radiative ($C_{\rm rad}$), van der Waals ($C_{\rm vdW}$), and Stark ($C_{\rm Stk}$) broadening. We assume that the absorption coefficient for each line has a Voigt profile given by

$$\phi_\nu = \frac{a}{\pi^{3/2}\Delta\nu_{\rm D}} \int_{-\infty}^{\infty} \frac{e^{-x^2}\,dx}{a^2 + [x - (\nu - \nu_0)/\Delta\nu_{\rm D}]^2}\,, \qquad (2)$$

where $\Delta\nu_{\rm D}$ is the Doppler width and a is the Voigt parameter

$$a = \frac{C_{\rm rad} + C_{\rm VdW}(n_{\rm H\,I}/10^{16})(T/5000)^{0.3} + C_{\rm Stk}(n_e/10^{12})}{\Delta\lambda_{\rm D}}\,. \qquad (3)$$

Here $n_{\rm H\,I}$ and n_e are the atomic hydrogen and electron densities, T is the electron temperature, and the Doppler width $\Delta\lambda_{\rm D} = (\lambda/\nu)\Delta\nu_{\rm D}$ is in units of Å. We have calculated $C_{\rm rad}$ according to Mihalas (1970), and the Stark broadening parameters were taken from Griem (1974). The van der Waals damping constants were computed following Deridder & Van Rensbergen (1976). For the 6–3 and 6–2 lines, we used the measured Stark and van der Waals widths given by Meyer & Beck (1970), instead of the computed values.

Collisional excitation rates are given by

$$C_{lu} = n_e\,\Omega_{lu}(T)\,\exp\left(\frac{-h\nu_{ul}}{kT}\right). \qquad (4)$$

Our values for $\Omega_{lu}(T)$ are given in Tables 2 and 3 for the optically allowed and forbidden transitions, respectively.

The rates for the allowed transitions were computed using Van Regemorter's (1962) formula. The forbidden transitions, on the other hand, where computed assuming an Einstein coefficient of 10^5 s^{-1} and using Van Regemorter's formula.

VAL76 computed these coefficients in a similar way, with the exception of the ones between the three lowest levels, which were scaled from C I values by Smith, Henry, & Burke (1967). We prefer to follow a unique criterion for all levels, considering that the VAL76 values were not obtained

[2] http://physics.nist.gov.

TABLE 2

ATOMIC PARAMETERS FOR RADIATIVE BOUND-BOUND TRANSITIONS

LINE	A_{ul} (s^{-1})	λ (Å)	C_{rad} (Å)	C_{vdW} (Å)	C_{Stk} (Å)	Ω_{lu} ($cm^3\ s^{-1}$) 3000 K	5000 K	7000 K	9000 K
4–1*	4.40(3)[a]	3009.75	1.05(−9)	1.03(−4)	...	1.38(−14)	1.57(−14)	1.75(−14)	1.75(−14)
5–1	1.74(8)[a]	2519.01	2.93(−5)	1.14(−4)	4.08(−7)	1.58(−08)	1.58(−08)	1.93(−08)	2.01(−08)
5–2	7.46(5)[a]	2979.92	4.13(−5)	1.63(−4)	...	2.20(−10)	2.48(−10)	2.78(−10)	2.79(−10)
5–3*	5.33(4)[a]	4102.94	7.79(−5)	2.87(−4)	...	2.41(−10)	3.04(−10)	3.03(−10)	2.97(−10)
6–1	2.03(6)[a]	2445.54	3.20(−5)	1.20(−4)	...	5.54(−11)	5.54(−11)	6.70(−11)	7.05(−11)
6–2	1.89(8)[a]	2882.48	4.47(−5)	1.07(−3)	3.11(−6)	1.65(−08)	1.82(−08)	2.08(−08)	2.10(−08)
6–3	1.18(7)[a]	3905.52	8.22(−5)	1.80(−4)	8.80(−7)	1.49(−08)	1.87(−08)	1.89(−08)	1.82(−08)
7–1	5.53(7)[a]	2214.77	7.16(−6)	7.60(−5)	...	5.34(−09)	5.34(−09)	6.17(−09)	6.71(−09)
7–2*	8.47(3)[b]	2564.26	9.65(−6)	1.07(−4)	...	2.46(−12)	2.46(−12)	3.02(−12)	3.13(−12)
7–3*	1.32(3)[b]	3344.03	1.64(−5)	1.95(−4)	...	4.85(−12)	5.82(−12)	6.19(−12)	6.08(−12)
8–5*	7.40(4)[b]	13400.62	8.68(−4)	4.85(−3)	...	1.00(−09)	1.06(−09)	1.17(−09)	1.20(−09)
8–6	8.10(6)[a]	15893.05	1.42(−3)	7.39(−3)	1.69(−4)	6.28(−07)	6.64(−07)	7.14(−07)	7.05(−07)
9–1*	1.07(5)[c]	2118.62	5.22(−6)	6.93(−5)	...	2.95(−12)	2.95(−12)	3.32(−12)	3.68(−12)
9–2	4.40(7)[c]	2435.94	6.95(−6)	9.30(−5)	...	3.55(−09)	3.55(−09)	4.29(−09)	4.52(−09)
10–5	1.69(7)[a]	11917.87	7.29(−4)	4.08(−3)	2.75(−5)	7.16(−07)	8.09(−07)	8.59(−07)	9.04(−07)
10–6*.....	9.37(3)[b]	14064.09	1.14(−3)	6.15(−3)	...	2.29(−09)	2.37(−09)	2.66(−09)	2.69(−09)
11–5	2.24(7)[a]	10760.78	5.75(−4)	3.66(−3)	1.39(−5)	4.06(−07)	4.49(−07)	4.56(−07)	4.97(−07)
11–7	2.45(6)[b]	26353.68	1.25(−3)	3.50(−2)	...	7.05(−07)	7.57(−07)	9.28(−07)	1.00(−06)
12–5	2.38(7)[a]	10440.10	5.62(−4)	3.55(−3)	3.18(−5)	1.30(−07)	1.43(−07)	1.43(−07)	1.58(−07)
13–1*.....	1.00(5)	2010.40	1.77(−8)	8.17(−5)	...	9.63(−12)	9.63(−12)	9.63(−12)	1.19(−11)
13–2*.....	4.52(4)[b]	2293.97	2.32(−8)	1.07(−4)	...	1.24(−11)	1.24(−11)	1.46(−11)	1.57(−11)
14–5*.....	3.73(4)[b]	9588.73	4.88(−4)	3.31(−3)	...	2.55(−10)	2.74(−10)	2.76(−10)	2.99(−10)
14–6	2.30(7)[a]	10872.72	7.11(−4)	4.39(−3)	2.18(−5)	7.20(−07)	7.98(−07)	8.14(−07)	8.84(−07)
15–1	8.33(7)[c]	1982.71	6.88(−6)	8.48(−5)	...	2.60(−09)	2.60(−09)	2.60(−09)	3.18(−09)
15–2*.....	1.06(5)[b]	2260.73	8.97(−6)	1.12(−4)	...	1.19(−11)	1.19(−11)	1.39(−11)	1.50(−11)
15–3*.....	8.96(3)[d]	2843.22	1.42(−5)	1.80(−4)	...	1.12(−11)	1.12(−11)	1.41(−11)	1.42(−11)
16–5*.....	6.79(4)[b]	8437.75	3.87(−4)	2.91(−3)	...	6.00(−11)	6.18(−11)	6.47(−11)	6.58(−11)
16–6	2.70(7)[a]	9416.26	5.45(−4)	3.72(−3)	2.86(−5)	1.04(−07)	1.11(−07)	1.13(−07)	1.21(−07)
17–1	5.00(6)[c]	1881.89	2.83(−5)	1.10(−4)	...	1.27(−10)	1.27(−10)	1.27(−10)	1.53(−10)
17–2	2.98(8)[c]	2124.83	3.63(−5)	1.41(−4)	...	2.09(−08)	2.09(−08)	2.36(−08)	2.61(−08)
18–1	4.18(6)[c]	1876.66	1.14(−5)	1.09(−4)	...	4.52(−11)	4.52(−11)	4.52(−11)	5.43(−11)
18–2	7.10(6)[c]	2123.70	1.46(−5)	1.41(−4)	...	2.13(−10)	2.13(−10)	2.40(−10)	2.66(−10)
18–3	1.06(8)[c]	2632.12	2.24(−5)	2.19(−4)	...	3.37(−08)	3.37(−08)	4.17(−08)	4.30(−08)
18–8	4.88(6)[b]	16384.96	9.30(−4)	1.01(−2)	...	4.23(−07)	4.51(−07)	4.79(−07)	4.87(−07)
19–1	2.35(8)[d]	1849.05	2.16(−5)	1.19(−4)	...	1.21(−08)	1.21(−08)	1.21(−08)	1.44(−08)
19–2	1.35(6)[d]	2086.98	2.77(−5)	1.55(−4)	...	1.90(−10)	1.90(−10)	2.12(−10)	2.37(−10)
19–3*.....	1.65(4)[d]	2575.57	4.21(−5)	2.37(−4)	...	2.43(−11)	2.43(−11)	2.99(−11)	3.10(−11)
19–10.....	3.18(5)[b]	16421.94	1.83(−3)	1.11(−2)	...	2.78(−08)	2.96(−08)	3.14(−08)	3.21(−08)
19–11.....	2.35(6)[b]	19420.48	2.54(−3)	1.59(−2)	...	6.22(−07)	6.87(−07)	6.91(−07)	8.23(−07)
20–1	8.16(7)[b]	1842.88	8.25(−6)	4.17(−4)	...	2.48(−09)	2.48(−09)	2.48(−09)	2.96(−09)
20–3	1.41(6)[d]	2569.46	1.61(−5)	7.84(−4)	...	1.24(−09)	1.24(−09)	1.52(−09)	1.57(−09)
20–10.....	6.81(6)[a]	16212.40	7.34(−4)	3.16(−2)	6.97(−5)	3.40(−07)	3.62(−07)	3.86(−07)	3.88(−07)
20–11.....	1.81(6)[b]	19002.63	9.94(−4)	4.13(−2)	...	2.66(−07)	2.93(−07)	2.97(−07)	3.48(−07)
21–1	2.48(6)[b]	1825.82	7.57(−6)	4.41(−4)	...	2.43(−11)	2.43(−11)	2.43(−11)	2.89(−11)
21–2	4.90(7)[b]	2058.83	9.66(−6)	5.62(−4)	...	1.32(−09)	1.32(−09)	1.45(−09)	1.63(−09)
21–3	2.45(7)[d]	2533.19	1.46(−5)	8.51(−4)	...	6.82(−09)	6.82(−09)	8.34(−09)	8.68(−09)
21–8	4.05(6)[b]	13180.74	4.34(−4)	2.31(−2)	...	1.54(−07)	1.65(−07)	1.81(−07)	1.86(−07)
21–14.....	5.86(6)[b]	21360.42	1.32(−3)	6.02(−2)	...	7.76(−07)	8.70(−07)	9.02(−07)	1.09(−06)

[a] Wiese & Fuhr 1999.
[b] Vienna Atomic Line Database.
[c] O'Brien & Lawler 1991.
[d] Smith et al. 1987.

specifically for Si I. Their values are a factor of 2 larger than ours for transitions 2–1 and 3–1 and similar to ours for the 3–2 transition.

Thus, many of the collisional rates are, at best, rough estimates. Since collisional processes affect the solution of the statistical equilibrium equations in an indirect way, except in the deep atmosphere where the atom is in LTE, we feel that the results obtained in this work have a greater reliability than such collision rate uncertainties. We discuss this point further in § 4.

TABLE 3

ATOMIC PARAMETERS FOR NONRADIATIVE BOUND-BOUND TRANSITIONS

This table is available only on-line as a machine-readable table.

3. THE INFLUENCE OF THE DIFFERENT LEVELS

In this section we study the influence of the different levels on the emitted profiles of the 6–3 and 5–3 transitions, at 3906 and 4103 Å, respectively. To do so, we compute the profile of this line for model C of Vernazza et al. (1981), as modified in the temperature minimum region by Avrett (1985; see also Maltby et al. 1986), and compare it with the observations reported in the Fourier Transform Spectroscopy (FTS) atlas of disk center intensity by Brault & Neckel (Neckel 1999). The T-versus-z distribution of the model we use is shown below in Figure 4 (*top panel*), for the lowest part of the atmosphere, which is of interest here.

The calculations were done using the computer code Pandora, kindly provided by E. H. Avrett (see Avrett & Loeser 1992 for an explanation of the program). An important feature that must be taken into account in every profile synthesis is the line blanketing due to a very large number of weak atomic and molecular lines. This effect is particularly important in the spectral region where the Si line is found, where there is such a large number of lines that it is not possible to determine the intensity of the "true continuum." In this work we included the 58×10^6 atomic and molecular lines computed by Kurucz (1991), in the way explained in Avrett, Machado, & Kurucz (1986) and Falchi & Mauas (1998).

In Figure 3 we show the computed profiles for both lines and compare them with the observations. It can be seen that this is a spectral region with a large number of weak lines contributing to the line blanketing, a fact that makes it difficult to determine the continuum level. In particular, to the blue side of the 4103 Å line the red wing of Hδ can be noticed.

In the second and third panels of Figure 4 we show the line source function and the Planck function for the 3906 and 4103 Å lines, which correspond to transitions 6–3 and 5–3, respectively. We also show the depth of formation of the radiation at different wavelengths from line center, marked with arrows in Figure 3, and of the "continuum" nearby. These depths of formation are given for two different values of μ (= cos Θ).

It can be seen that both source functions decouple from the Planck function and become larger than it, very deep in the atmosphere, below the temperature minimum region. This fact can be understood with the help of Figure 4 (*bottom panel*), similar to Figure 24 of VAL76. In this figure we show the departure coefficients b_l for the three lowest levels and for levels 5 and 6, which are the upper levels of the transitions of interest here. The departure coefficients are defined such that $n_l/n_k = b_l\, n_l^*/n_k^*$.

It can be seen that the three lowest levels are strongly coupled, and therefore their departure coefficients remain very similar throughout the region where the lines are formed (Fig. 4, *second and third panels*). As a result of overionization of these low levels, their b values become smaller than unity at around 200 km, while b_5 and b_6 are much closer to unity. Therefore, the source function for these lines, which can be approximated as

$$S_\nu = \frac{b_u}{b_3} B_\nu \quad (u = 5, 6)\,, \tag{5}$$

becomes larger than the Planck function.

To compare the effect that different levels have on the degree of ionization, we computed $\mathscr{R}_{lk}$, the net rate of ionization from level l as a function of depth, normalized (for convenience in plotting) by the factor b_1/n_1. $\mathscr{R}_{lk}$ is, therefore, defined as

$$\mathscr{R}_{lk} = (n_l R_{lk} - n_k R_{kl}) \frac{b_1}{n_1}\,, \tag{6}$$

where b_1 is the departure coefficient for the ground level and R_{lk} and R_{kl} are the photoionization and photorecombination rates, respectively, given by

$$R_{lk} = 4\pi \int_{\nu_{kl}}^{\infty} \frac{1}{h\nu}\, \alpha_l(\nu) J_\nu\, d\nu\,, \tag{7}$$

$$R_{kl} = \frac{n_l^*}{n_k^*}\, 4\pi \int_{\nu_{kl}}^{\infty} \frac{1}{h\nu}\, \alpha_l(\nu) e^{-h\nu/kT} \left(\frac{2h\nu^3}{c^2} + J_\nu \right) d\nu\,. \tag{8}$$

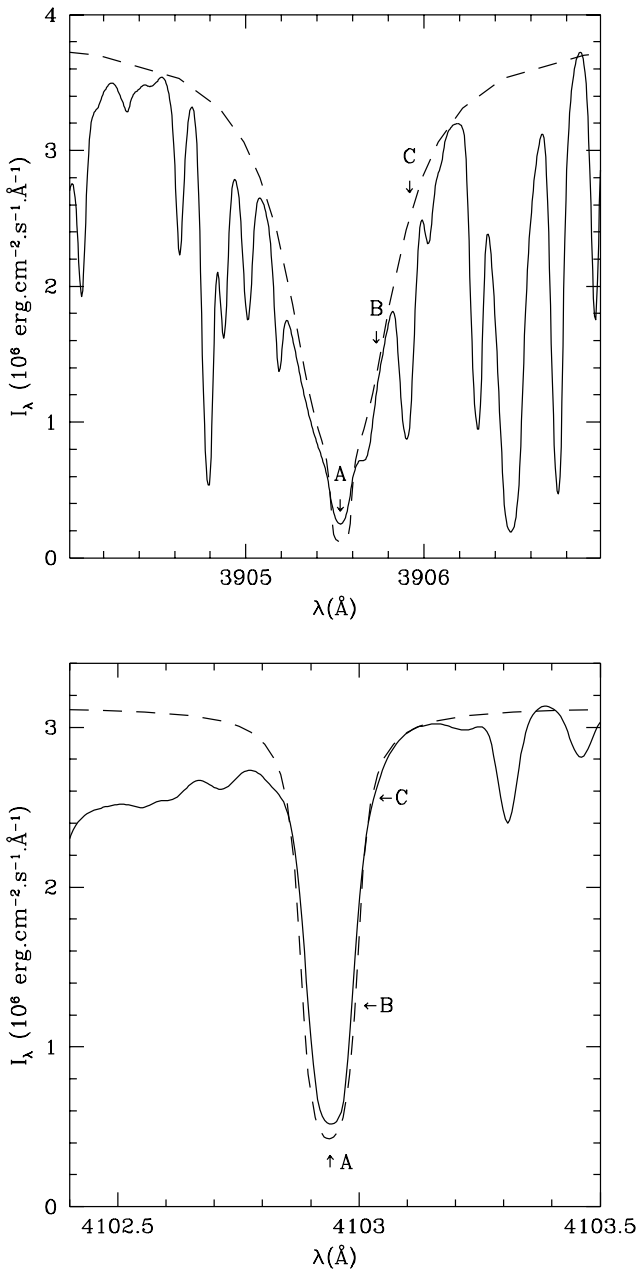

FIG. 3.—Computed (*dashed line*) and observed (*solid line*) profiles. The arrows indicate the wavelengths for which the height of formation is shown in Fig. 4 (*second and third panels*).

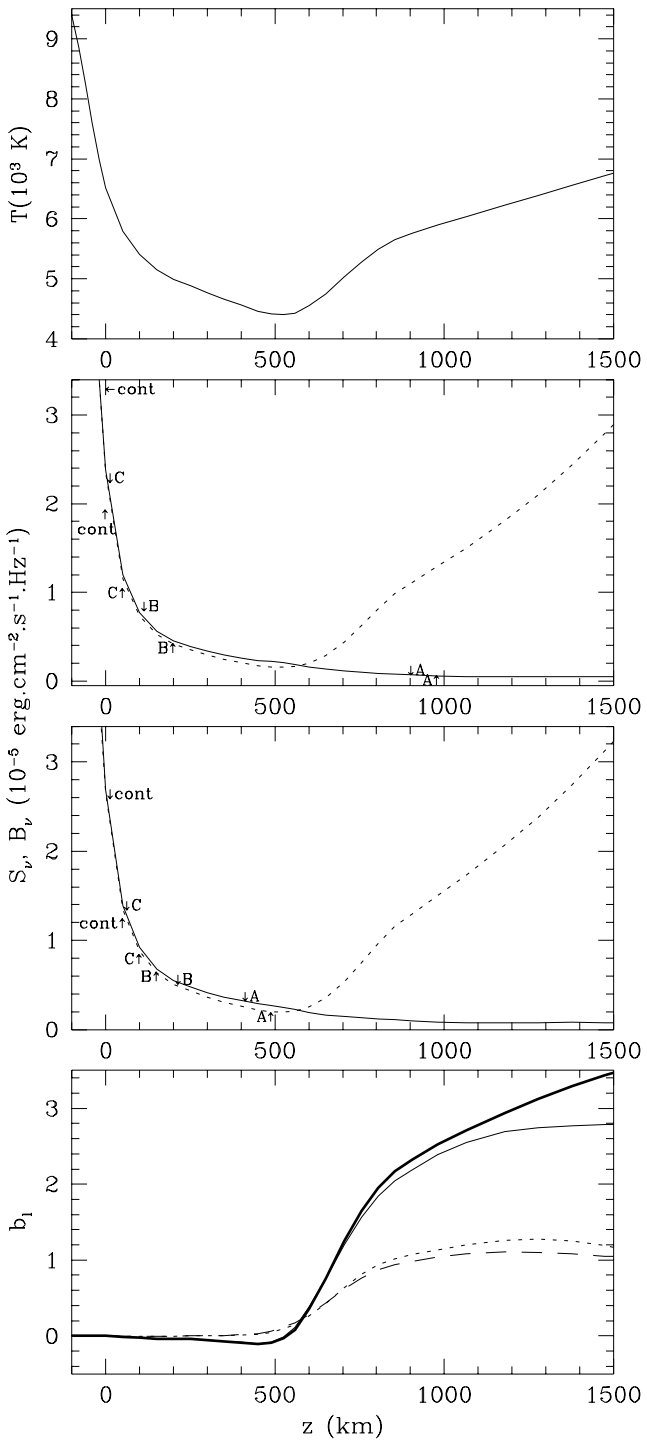

FIG. 4.—*Top panel:* Atmospheric model used here. *Second panel:* Source (S_ν, *solid line*) and Planck (B_ν, *dotted line*) functions for the 6–3 transition. The arrows show the height of formation of the radiation at the wavelengths indicated in Fig. 3. The values at disk center are indicated above the S_ν curve, and those at $\mu = 0.4$ are indicated below it. *Third panel:* Same, but for the 5–3 transition. *Bottom panel:* Departure coefficients b_l for several levels. *Thick solid line:* levels 1 and 2. *Thin solid line:* level 3. *Dotted line:* level 5. *Dashed line:* level 6. Note that $b_2 = b_1$.

The thermodynamic equilibrium ratio n_l^*/n_k^* is given by the Saha-Boltzmann relation

$$\frac{n_l^*}{n_k^*} = n_e \left(\frac{h^2}{2\pi m k T}\right)^{3/2} \frac{g_l}{2U_k} e^{h\nu_{kl}/kT}, \qquad (9)$$

where U_k is the partition function for Si II. Statistical equilibrium requires that $\sum_l \mathcal{R}_{lk} = 0$.

In Figure 5 we show the net ionization rates $\mathcal{R}_{lk}$ as a function of depth for those levels that are important in the ionization balance.

It can be seen that, in the region of interest, ionization takes place mainly from the second level, while recombination occurs to the highest levels, in particular to levels 10, 11, and 13. It is, therefore, necessary to include these high levels to account for the ionization balance accurately. We will return to this point in § 6, when discussing the influence that the radiation coming down from the transition region has on the ionization equilibrium.

4. THE OPTIMUM MODEL

Since the present atomic model will be used for chromospheric modeling and, in particular, to study the velocity fields in the chromosphere, it is very important to find a valid approximation that includes the minimum possible number of transitions, to avoid large computing times.

For each spectral line considered, the transfer equation has to be solved for a number of frequencies, typically of around 30. When the velocity fields are included, the number of frequencies is automatically doubled, since the lines are not symmetric any more. Furthermore, since the frequencies are Doppler shifted by a different amount at each depth, the number of frequencies to work with increases by an additional factor of n, the number of depth points in the grid.

We therefore tried different models with reduced numbers of transitions and found that a model not including the lines with Einstein coefficients $A_{ul} \leq 10^5$ s^{-1} results in the same profiles for the two lines of interest, with a 30% gain in computing time.

On the other hand, we compute the bound-free rates integrating on a fixed number of wavelengths, which are the same for all levels. Therefore, the number of levels is not as important in determining the computing time as the number of lines.

For example, we made a calculation with a 20 level atomic model, not including level 4 of the standard model. We expected that this change would not affect our calculations since, on the one hand, the net ionization rate for this level can be neglected compared to the rates to the other levels, as was pointed out in § 3, and on the other hand, the only transition coupling this level to other levels is the 4–1 transition, with $A_{41} = 4.4 \times 10^3$ s^{-1}, which was therefore not included in the reduced model mentioned above. The calculations with this 20 level model gave, indeed, the same results as before, but the gain in computing speed was of only 2%. We feel that, in view of this fact, it is not worth reducing the number of levels.

In this way, we arrive at what can be called an "optimum model," in the sense that it includes all the atomic processes that can affect the profiles of the lines under study, being at the same time the one with the smallest number of transitions needed and thus the fastest to compute. The lines not included in this model are the ones marked with a dashed line in Figure 1 and with an asterisk in Table 2.

5. INFLUENCE OF THE ATOMIC PARAMETERS

We have investigated the influence that a change of the different atomic parameters has either on the computed

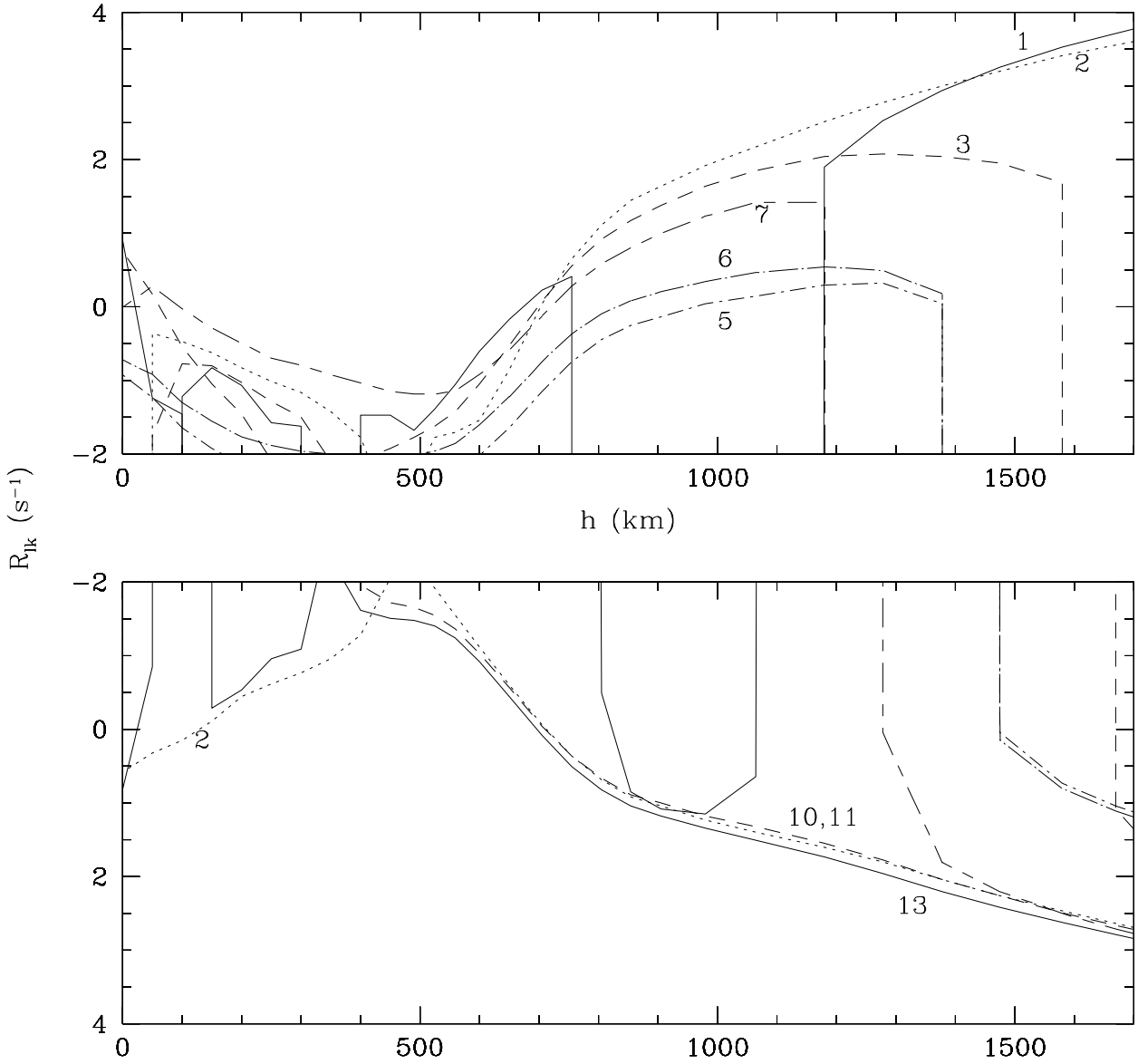

FIG. 5.—Net photoionization rate $\mathscr{R}_{lk}$ for several levels of the atomic model. A positive rate implies net ionization, and a negative rate implies net recombination.

populations of the atomic levels or on the profiles of the lines under study, as a way to estimate how the uncertainty on these parameters is reflected in the computed profiles. The results of these calculations are presented in this section.

5.1. *Photoionization Cross Sections*

As pointed out in § 2.1, the photoionization cross sections adopted here are very different from those adopted previously by VAL76. In particular, the threshold value of the cross section for level 1 used by VAL76 is 37 mbar, almost half the one obtained here. Furthermore, the variation of the cross section with wavelength is also very different.

We therefore made a trial run using the VAL76 value for the cross section of the ground state. We found that the degree of ionization only changes noticeably above 1500 km, where $\mathscr{R}_{1k}$ becomes important (see Fig. 5). However, at this height the lines are already optically thin, and therefore the profile does not change.

Keeping in mind that, as can be seen in Figure 5, $\mathscr{R}_{2k}$ is the most important contribution to the ionization, we tried the VAL76 cross section for this level, which has the same threshold value, although it does not include the resonances. In this case there is a slight change in the degree of ionization, but it is only of about 5% in the region where the lines are formed, and it does not affect the computed profiles. We also tried a model with the VAL76 photoionization cross sections for the seven lowest levels, and also in this case we found almost no differences in the populations or in the emitted profiles.

The modification of the cross sections of the highest levels has a larger effect. We tried multiplying by 2 the cross sections for levels 9–21 and found that this resulted in an increase in the population of the lowest levels by as much as

15%, since, as shown in Figure 5, recombination is dominated by these levels, in particular by level 13.

The fact that these lines are not affected by these changes in the parameters is an advantage when using the profiles as chromospheric diagnostics, since the conclusions are not affected by indeterminations in the atomic parameters.

5.2. *Collisional Cross Sections*

As explained in § 2, the collisional cross sections are the parameters in these calculations that have the largest uncertainties. Furthermore, we have neglected the collisions with atomic hydrogen, which have been proposed as an important process to take into account for profile synthesis. For example, Lemke & Holweger (1987) and Baumüller & Gehren (1996) included them in studies of Mg I and Al I lines, respectively. Andretta, Doyle, & Byrne (1997) also considered collisions with H in their calculation of Na D profiles in dM stars and found that the effect of these collisions is not important for the emerging profiles.

These collisions can be particularly important for the lines under study here, which form around the $T_{\rm min}$, where neutral hydrogen is 10^4 times more abundant than free electrons. To assess the importance of this possible source of error in our computations, in this section we explore the influence that variations on the collisional rates can have on the observed profiles.

We first increased by a factor of 10 the collisional ionization cross sections for the first 10 levels and found that the total influence of this change did not affect the level populations by more than 5% in the lower chromosphere, since radiative bound-free processes are much more effective than collisional ones. Increasing the collisional rates for the remaining levels did not have any effect at all. One of the less reliable approximations we made was to set the cross section for nonradiative bound-bound transitions equal to the ones for an allowed transition with the same energy difference and a value of the Einstein coefficient $A_{ji} = 10^5$ s^{-1}.

We first made a trial run increasing the cross sections between the three lowest levels by a factor of 3. In this case, the population of level 3 increases by 10% in the region of formation of the center of the line at 3906 Å, as a result of a stronger coupling with the two lowest levels (see Fig. 4). However, since the population of level 6 is collisionally coupled to the ones of the lowest levels, it also increases, and the source function of the 6–3 line does not vary, keeping the line profile unchanged. The 5–3 line does not change either, since it is formed deeper in the atmosphere, and it is already very close to LTE with the original values of the cross sections. The other rates have less influence, and increasing the collisional rates for all nonradiative transitions had no further effect.

A much larger change in the populations results if another criterion is used to compute the cross sections of the forbidden lines. In a study of the Mg I lines, Mauas, Avrett, & Loeser (1988) computed these cross sections assuming a fixed oscillator strength of 0.1 in Van Regemorter's formula, instead of a fixed value for the Einstein A_{ul}. This criterion results in larger values for the collision rates between levels with smaller energy difference. If this is done, the three lowest levels become completely coupled, and the population of level 3 increases by 25% where the 6–3 line center is formed. However, the population of level 6 also increases, and the profile of the 6–3 line is affected only in the line center, resulting in a 20% lower intensity, with the residual intensity going from 0.029 to 0.022. The contrast between continuum and central intensity, on the other hand, changes only from 0.971 to 0.978 and is barely noticeable in the line plots.

But not only the collisional rates for the forbidden transitions are uncertain. The Van Regemorter formula was also used for the optically allowed transitions, since no experimental values for the cross sections are available. To check if this approximation can affect the resulting profiles, we made two trial runs multiplying by 3 the cross sections for the 6–3 and 5–3 transitions, corresponding to the lines under study, and found no changes in the line profiles.

5.3. *The Einstein Coefficients*

The Einstein coefficients of the lines under study have, in principle, a strong influence on the computed profiles, since they determine the depth of formation of the line. In fact, we can express the optical depth in the center of a line with lower and upper levels l and u, respectively, at the geometrical depth z as

$$\tau_0 = \left(\frac{h\nu}{4\pi}\right) B_{lu} \left(N_l - N_u \frac{g_l}{g_u} \right), \tag{10}$$

where B_{lu} is the Einstein coefficient for direct absorption, related to the A_{ul} listed in Table 2 by

$$B_{lu} = \frac{c^2}{2h\nu_{ul}^3} \frac{g_u}{g_l} A_{ul} . \tag{11}$$

In these equations, g_l and g_u are the statistical weights of the levels and N_l and N_u are the column number densities, or the number of atoms in each level per unit area above z, i.e., $N_i(z) = \int_z^\infty n_i(z')dz'$, where n_i is the number density of atoms in level i. In equation (10), the second term inside the second set of parentheses accounts for stimulated emission and can be neglected for the lines considered here.

As explained in § 2.2, the values of A_{ul} found in the literature can differ typically by 50%, but the situation is not so critical for the lines under study here. We made a run with the highest value of A_{63} found in the literature and found no differences in the computed profile. This is due to the fact that the source function in the region of formation of this line is quite flat, and therefore changing by a few kilometers the region of formation of the line does not alter the emitted intensity.

On the other hand, if A_{53} is changed to the lowest value given by VALD, the computed central intensity increases slightly, reducing the difference between observed and computed values to half of what is observed in Figure 3. However, the very good agreement seen in the wings is destroyed. We therefore believe that the NIST value used here is a better choice for this parameter.

5.4. *Damping Parameters*

We have found that van der Waals broadening is the main factor in determining the 6–3 Voigt parameter (eq. [3]) in the region of formation. As can be seen in Figure 3, the adopted experimental value of 1.8×10^{-4} Å fits very well the observations. The value obtained following Deridder & Van Rensbergen (1976), as was done for the remaining transitions, is 2.8×10^{-4} Å. This value is clearly too large and results in a line much broader than observed.

The experimental value for the 6–2 C_{vdW} is, on the other hand, 8 times larger than the computed one. We checked with the smaller value and found that this change had no effect on the computed profiles of the 6–3 and 5–3 lines.

The profile of the much narrower 5–3 line, on the other hand, is dominated by Doppler broadening, and only in the wings does van der Waals broadening become important. For this line the computed C_{vdW} fits quite well the observed profile, but an increase of a factor of 2 in C_{vdW} only marginally worsens the fit. Changes on the Stark widths C_{Stk}, on the other hand, do not change the computed profiles.

5.5. *Opacities*

Although rather insensitive to variations in the Si I atomic parameters, the line profiles are strongly dependent on the sources of continuum opacities included in the calculations. Here we have considered, in addition to Rayleigh and electron scattering, the absorptions due to H^-, H, H^{2+}, He, He II, Mg, C, Al, Fe, Na, and Ca, as well as Si itself, and all these contributions were obtained from non-LTE computed populations. As explained in § 3, we have also included the contribution due to weak atomic and molecular lines compiled by Kurucz (1991) in the way explained by Falchi & Mauas (1998).

As this method treats the opacity in a statistical way, it is appropriate to compute the photoionization rates, which depend on the integral of the radiation, and to give an approximate idea of the continuum level, but it does not reproduce the exact radiation field at a precise wavelength. For example, it does not reproduce the continuum level in the far wings of the lines under study.

We therefore had to modify the amount of line blanketing, increasing it by 30% at the wavelength of the 5–3 line and reducing it by a factor of 5 for the 6–3 line. In the latter case, the line blanketing probably included the contribution of the silicon line we were recomputing explicitly. As can be seen in Figure 3, with this method it is not possible to reproduce the continuum in detail; in particular, the wing of Hδ to the blue side of the 4103 Å line is not reproduced. Nevertheless, it does provide a good fit to the line profiles.

Although these opacities, and the ad hoc adjustment we had to make, do not affect the intensity at line center, it does affect the residual intensity because it changes the continuum level. Therefore, residual intensities should be used with caution when comparing with the observations. For a more thorough discussion of this and other effects that can affect the atmospheric modeling, see Falchi & Mauas (1998).

To study the influence of these weak-line opacities in the ionization of Si I, we recomputed the model using the average line opacity distribution of VAL76 in the ionization continua of the levels. The effect on the overall ionization balance was smaller than 5% in the region of interest, by contrast to the case of Mg I studied by Mauas et al. (1988). The profiles did not change at all.

6. LINE IRRADIATION

As mentioned in § 1, several authors have discussed the fact that ionization of Si I can be affected by the irradiation from UV lines coming down from the upper chromosphere or the transition region (TR) and that this irradiation can alter the continuum intensity below 1682 Å, the ionization threshold of level 2 of Si I. In this section we follow on with these studies and address the question of how much influence this radiation may have on the line profiles.

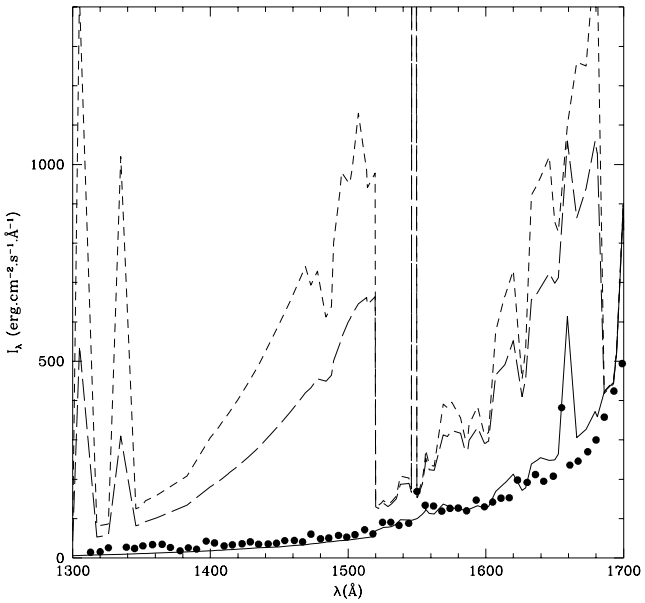

FIG. 6.—Continuum emission at disk center. *Solid line:* Without irradiation. *Long-dashed line:* Umbra irradiation. *Short-dashed line:* Plage irradiation. *Filled circles:* Observations by Kohl et al. (see VAL76).

In Figure 6 we show the continuum radiation computed from our model and compare it with the observations by Kohl, Parkinson, & Reeves listed in VAL76. It can be seen that there is good agreement between the observed and computed values. We have checked whether the computed continuum varies when the photoionization cross sections are changed and found that if the VAL76 cross sections are used, the computed emitted intensity is slightly lower, with the maximum change of around 10% occurring at 1640 Å.

Several TR lines can affect the ionization equilibrium of Si around the T_{min}. A detailed list can be found in Sandlin et al. (1986), who give line intensities for the quiet Sun, a plage, and a sunspot umbra. Here we have included the strongest lines from their list, which are given in Table 4. We have considered for all the lines an indicative FWHM of 0.15 Å, to estimate the fluxes.

TABLE 4

CENTRAL INTENSITIES OF THE UV LINES CONSIDERED (FROM SANDLIN ET AL. 1986)

Wavelength	Species	Plage[a]	Umbra[a]	Quiet[a]
1206.511.....	Si III	52.2	6.4	4.0
1218.351.....	O V	5.3	16.2	0.4
1238.824.....	N V	9.8	15.4	0.7
1302.170.....	O I	20.0	10.1	1.7
1304.860.....	O I	21.0	10.6	2.3
1306.028.....	O I	20.0	10.4	2.5
1334.535.....	C II	39.2	14.9	2.7
1335.708.....	C II	56.0	20.3	3.4
1393.760.....	Si IV	13.0	3.7	0.6
1526.708.....	Si II	10.5	0.6	0.8
1533.432.....	Si II	11.5	0.6	0.8
1548.190.....	C IV	16.5	8.4	0.9
1670.780.....	Al II	11.2	5.3	0.2

[a] Units are 10^3 ergs cm^{-2} s^{-1} Å^{-1}.

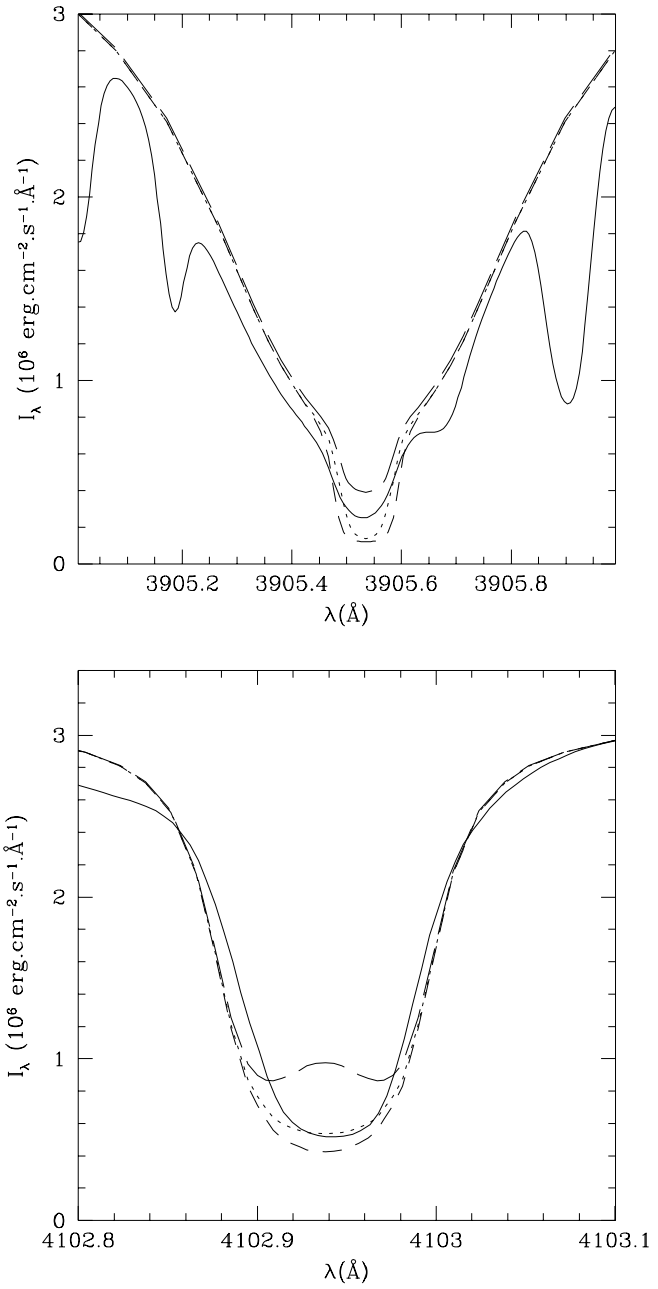

FIG. 7.—Detail of the line profiles. *Solid line:* Observations. *Short-dashed line:* Without irradiation. *Dotted line:* Plage irradiation. *Long-dashed line:* Plage irradiation enhanced by 10^3 to simulate the flare irradiation.

We made two trial runs, assuming incident radiation of the levels listed in Table 4 for the plage and the sunspot umbra. In these calculations we considered that the line radiation is incident on the most external point of our grid, which is placed at the top of the TR, at 10^5 K. This radiation is affected by the sources of opacity mentioned in § 5.5, and therefore only a fraction of it reaches the $T_{\rm min}$ region, where the continuum is formed. The Si I equilibrium is computed consistently with this incident radiation.

The resulting continua are also shown in Figure 6. It can be seen that these results confirm the previous calculations and that TR irradiation does indeed increase strongly the emitted continuum at this wavelength, since it strongly changes the degree of ionization of Si I. In fact, when the radiation is included, ionization from the ground state is strongly enhanced, and $\mathcal{R}_{1k}$ becomes positive everywhere in the atmosphere and larger than $\mathcal{R}_{2k}$.

However, since the equilibrium between the bound levels is largely independent of the degree of ionization, the irradiation affects much less the emitted profiles, as can be seen in Figure 7, where we compare the profiles computed with the plage fluxes with the ones obtained with no irradiation. However, one should keep in mind that during flares the TR lines are largely enhanced. For example, the flux used here for the C IV line at 1549 Å in a plage is 2.5×10^3 ergs cm^{-2} s^{-1} sr^{-1}, while Machado & Hénoux (1982) give a value of 4×10^5 ergs cm^{-2} s^{-1} sr^{-1} for the decay phase of a flare, and Machado & Mauas (1986) give values between 1 and 5×10^6 ergs cm^{-2} s^{-1} sr^{-1} for the impulsive phase of a flare.

In Figure 7 we also show the profiles obtained with an irradiating flux equal to 10^3 times the one used for the plage, a level that can be considered representative of the situation during flares. It can be seen that in this case, the line profiles are quite different, even if the atmosphere is not altered. This effect could be even larger in a flaring atmosphere, where the lines are seen in emission (Cauzzi et al. 1996).

Therefore, if the Si line profiles are to be used as a diagnostic of the chromospheric structure during flares, one should carefully take into account the irradiation by TR lines and the sources of opacity that can affect it.

7. CONCLUSIONS

We have compiled a reliable atomic model for profile calculations of two Si I lines in the blue region of the spectrum. We found that it is necessary to include several high-energy levels to obtain an accurate treatment of the ionization balance. The eight-level model used by VAL76 and subsequent papers may be, therefore, inappropriate. On the other hand, we found that it is not necessary to compute explicitly the radiative transitions for all the lines and that a model much faster to compute can be obtained if the lines with $A \leq 10^5$ s^{-1} are not considered.

We have studied the influence that the uncertainties in the values of the different atomic parameters may have on the calculated profiles and have found that both profiles are rather insensitive to these parameters, within the reasonable values to be expected. This characteristic is very important, since it makes these lines very reliable as chromospheric diagnostics.

Moreover, the 5–3 line is close to LTE throughout its region of formation, just below $T_{\rm min}$, and can therefore be used to determine the temperature structure at this depth. We also found that the NIST value for A_{53} fits better the observations than the one given in VALD.

We reassessed the importance that the irradiation by UV lines originating in the transition region has on the degree of ionization of Si and found that, as mentioned in different studies, this contribution is fundamental in solar kernels with different degrees of activity.

We also found that this irradiation can affect the line profiles during flares, where it is strongly enhanced. Therefore, to use these lines as diagnostics of the flaring chromosphere, the effect of the transition region lines should be explicitly taken into account.

REFERENCES

Andretta, V., Doyle, J. G., & Byrne, P. B. 1997, A&A, 322, 266
Asplund, M. 2000, A&A, 359, 755
Avrett, E. H. 1985, in Chromospheric Diagnostics and Modeling, ed. B. W. Lites (Sunspot: NSO), 67
Avrett, E. H., & Loeser, R. 1992, in ASP Conf. Ser. 26, Cool Stars, Stellar Systems, and the Sun: 7th Cambridge Workshop, ed. M. S. Giampapa & J. A. Bookbinder (San Francisco: ASP), 489
Avrett, E. H., Machado, M. E., & Kurucz, R. L. 1986, in The Lower Chromosphere of Solar Flares, ed. D. F. Neidig (Sunspot: NSO), 216
Baumüller, D., & Gehren, T. 1996, A&A, 307, 961
Becker, U., et al. 1980, Phys. Lett., 76, 125
Cauzzi, G., et al. 1995, A&A, 299, 611
———. 1996, A&A, 306, 625
Cram, L. E., & Mullan, D. J. 1979, ApJ, 234, 579
Cunto, W., et al. 1993, A&A, 275, L5
Deridder, G., & Van Rensbergen, W. 1976, A&AS, 23, 147
Doyle, J. G., & Phillips, K. J. H. 1992, A&A, 257, 773
Falchi, A., & Mauas P. J. D. 1998, A&A, 336, 281
———. 1999, in Magnetic Fields and Solar Processes (Noordwijk: ESA), 779
Freund, R. S., et al. 1990, Phys. Rev. A, 41, 3575
Ganas, P. S. 1999, A&AS, 138, 323
Giampapa, M. S., Worden, S. P., & Linsky, J. L. 1982, ApJ, 258, 740
Grevesse, N., et al. 1991, A&A, 242, 488
Griem, H. R. 1974, Spectral Line Broadening by Plasmas (New York: Academic Press)
Hibbert, A. 1979, J. Phys. (Paris), C1, Supp. 2, 40, 122
Hoffman, W. 1969, Z. Naturforschung, 24, 990
Houdebine, E. R., & Doyle, J. G. 1994, A&A, 289, 185
Iglesias, C. A., Rogers, F. J., & Wilson, B. G. 1992, Rev. Mexicana Astron. Astrofis., 23, 9
Kupka, F., Piskunov, N. E., Ryabchikova, T. A., Stempels, H. C., & Weiss, W. W. 1999, A&AS, 138, 119
Kurucz, R. L. 1991, in Precision Photometry: Astrophysics of the Galaxy, ed. A. G. Davis Philip, A. R. Upgren, & K. A. Janes (Schenectady: L. Davis Press), 441
Lemke, M., & Holweger, H. 1987, A&A, 173, 375
Machado, M. E., Avrett, E. H., Vernazza, J., & Noyes, R. W. 1980, ApJ, 242, 336
Machado, M. E., & Hénoux, J. C. 1982, A&A, 108, 61
Machado, M. E., & Mauas, P. J. D. 1986, in Rapid Fluctuations in Solar Flares, ed. B. R. Dennis, A. Kiplinger, & L. Orwig (Washington: NASA), 271
Maltby, P., et al. 1986, ApJ, 306, 284
Mauas, P. J. D. 1993, ApJ, 414, 928
———. 2000, ApJ, 539, 858
Mauas, P. J. D., Avrett, E. H., & Loeser, R. 1988, ApJ, 330, 1008
Mauas, P. J. D., & Falchi, A. 1994, A&A, 281, 129
———. 1996, A&A, 310, 245
Mauas, P. J. D., Falchi, A., Pasquini, L., & Pallavicini, R. 1997, A&A, 326, 249
Mauas, P. J. D., Machado, M. E., & Avrett, E. H. 1990, ApJ, 360, 715
Mendoza, C., & Zeippen, C. J. 1988, J. Phys. B, 21, 259
Meyer, J., & Beck, R. J. 1970, A&A, 8, 93
Mihalas, D. 1970, Stellar Atmospheres (San Francisco: Freeman)
Morton, D. C. 1991, ApJS, 77, 119
Mukherjee, P. K., & Ohno, K. 1989, Phys. Rev. A, 40, 1753
Nahar, S. N. 1993, Phys. Scr., 48, 297
Nahar, S. N., & Pradhan, A. K. 1993, Phys. Rev. A, 26, 1109
Neckel, H. 1999, Sol. Phys., 184, 421
O'Brien, T. R., & Lawler, J. E. 1991, Phys. Rev. A, 44, 7134
Piskunov, N. E., Kupka, F., Ryabchikova, T. A., Weiss, W. W., & Jeffery, C. S. 1995, A&AS, 112, 525
Ryabchikova, T. A., Piskunov, N. E., Stempels, H. C., Kupka, F., & Weiss, W. W. 1999, Phys. Scr., 83, 162
Saloman, E. B. 1990, Spectrochim. Acta, 45, 37
Sandlin, G. D., et al. 1986, ApJS, 61, 801
Savage, B. D., & Lawrence, G. M. 1966, ApJ, 146, 940
Smith, K., Henry, R. J. W., & Burke, P. G. 1967, Phys. Rev., 157, 51
Smith, P. L., et al. 1987, ApJ, 322, 573
Thatcher, J. D., Robinson, R. D., & Rees, D. E. 1991, MNRAS, 250, 14
Van Regemorter, H. 1962, ApJ, 136, 906
Vernazza, J. E., Avrett, E. H., & Loeser, R. 1973, ApJ, 184, 605
———. 1976, ApJS, 30, 1 (VAL76)
———. 1981, ApJS, 45, 635
Verner, D. A., Barthel, P. D., & Tytler, D. 1994, A&AS, 108, 287
Wiese, W. L., & Fuhr, J. R. 1999, NIST Atomic Spectra Database